ELSEVIER

Journal of Photochemistry and Photobiology A: Chemistry 109 (1997) 267–280

Journal of PHOTOCHEMISTRY AND PHOTOBIOLOGY A: CHEMISTRY

UV photon-assisted incineration of polycyclic aromatic hydrocarbons at elevated temperatures between 150 and 800 °C

Andreas Thöny, Michel J. Rossi *

Institute of Environmental Sciences/Laboratory for Air and Soil Pollution Studies (IGE/LPAS), Swiss Federal Institute of Technology—Lausanne (EPFL) CH-1015, Lausanne, Switzerland

Received 20 January 1997

Abstract

In this feasibility study we investigated the UV photon-assisted thermal decomposition of the title compounds. UV photons from an appropriate light source such as a laser or a lamp were combined with heat at modest temperatures in an incinerating flow reactor in order to obtain a more efficient decomposition of hydrocarbons. In model experiments we have achieved a destruction enhancement factor of the photon-assisted thermal compared with the pure thermal decomposition process in excess of 10^3. Comparing pyrene with 1-bromopyrene we were able to demonstrate that the efficiency of populating the lowest energy triplet state by intersystem crossing from the corresponding singlet state plays an important role in the photon-assisted thermal destruction in addition to the importance of the molecular absorption coefficient. The overall quantum yield for the photon-assisted thermal decomposition generally increases slightly with temperature but decreases with increasing photon flux. For some compounds we determined overall quantum yields exceeding unity thus pointing towards a possible photon-initiated chain reaction. Levels of destruction in the ppb range seem possible at moderate temperatures of less than 900 °C and gas phase residence times of only a few seconds. © 1997 Elsevier Science S.A.

Keywords: Hot photochemistry; UV-photo assisted incineration; Polycyclic aromatic hydrocarbons

1. Introduction

The proper disposal of the waste generated by our society is one of the main environmental problems of today. Of the large amounts of municipal and industrial waste, 7.7 billion tons are produced annually by the OECD countries. A few percent are classified as toxic or hazardous waste and require special disposal techniques [1]. Furthermore, there are important quantities of already existing toxic waste awaiting proper disposal. Therefore, the development of novel ways for the efficient disposal of toxic and municipal waste is an important task in view of increasing population density and world-wide industrial development. It appears highly desirable to enable alternative destruction technologies in addition to pure thermal incineration in order to fulfill today's regulations for the emission of remaining organic hydrocarbons from hazardous waste incinerators aiming at a destruction and removal efficiency (DRE) of 99.9999% for dioxin-listed and 99.99% for other organic waste compounds [2]. It is to be expected that such regulations will be even more restrictive in the near future and there may soon be a demand for more efficient and safer technologies. One of these potential new technologies may be to apply the principle laid out in this work, namely the combination of thermal decomposition and photochemistry.

In their search for a highly efficient and cost-effective disposal technology Graham and Dellinger [3] investigated the synergism between high temperature incineration and UV–visible radiation in a solar incinerator. They took selected organic compounds as surrogates for toxic organic waste in their photo-assisted destruction studies. They performed laboratory experiments using a powerful Xe arc lamp in combination with an air-mass filter to simulate solar radiation and predicted a large increase in the DRE of the photon-assisted thermal process compared with the purely thermal destruction for irradiation conditions approaching 1000 suns [4]. From field tests on 1,2,3,4-TCDD (tetrachloro-dibenzo-*p*-dioxin) in full scale solar incinerators at the White Sands Missile Range and at Sandia National Laboratory a photon-induced enhancement of up to a factor of 10^4 was reported by Glatzmaier et al. [5], leading to a fraction remaining f_r for this compound on the order of 10^{-6} at 750 °C corresponding to a DRE of 99.9999% which satisfies the requirements for the emission of dioxin-like compounds [2]. Equivalent

* Corresponding author.

PII S1010-6030(97)00150-0

DRE values can be obtained by traditional incineration technology only when heating to temperatures on the order of 1600 °C or more [3].

A more detailed laboratory study on the high-temperature photon-assisted oxidation of monochlorobenzene was published by Graham et al. [6]. They reported on the photon-assisted DRE using a pulsed dye laser at 280 nm and on the quantitative study of the products of the photooxidation process. This effort peaked in 1995 when Graham and Dellinger patented a method and an apparatus for photon-assisted thermal destruction of toxic organic compounds using lamps or lasers [7] and discussions are reportedly under way to build an initial full-scale unit equipped with six 15 kW Hg arc lamps [8].

We have chosen the approach to use either excimer lasers or arc lamps as an UV source for the photon-assisted thermal destruction of model organic compounds in a laboratory scale incinerator using a flow tube at atmospheric pressure having a constant sample inlet concentration [9,10]. The goal of our feasibility study is to investigate the destruction enhancement of the photon-assisted thermal over the purely thermal incineration from a fundamental point of view using the title molecules each representing classes of highly toxic polycyclic aromatic hydrocarbons (PAH). The results of this study should give some hints towards future applications of techniques aimed at a more efficient destruction in an incinerating unit of highly toxic compounds such as polychlorinated dibenzo-*p*-dioxins (PCDDs), polychlorinated dibenzofurans (PCDFs) and polychlorinated biphenyls (PCBs). We selected anthracene as a representative PAH being an innocuous species in order to establish the experimental technique. Furthermore, we have chosen xanthone as an additional example having an ether linkage and a carbonyl group between the two benzene rings, pyrene as a basic representative of PAHs with four benzene rings and its 1-substituted bromoderivative, as well as 1,2,4-trichlorobenzene as a representative of multiply substituted chlorine containing aromatic hydrocarbons.

2. Theoretical aspects

The detailed reaction mechanism of photon-assisted incineration is not yet completely understood. The activation energy for unimolecular decomposition occurring at a rate constant k_d' out of the first excited singlet state S_1 ($^1A^*$) presumably is significantly smaller compared with the ground electronic state S_0 (A in Fig. 1). However, in view of the short lifetime of S_1 in the nanosecond or sub-nanosecond range, it is more likely that reaction or decomposition occurs from the lowest metastable triplet state T_1 ($^3A^*$) formed by intersystem crossing from the primary photoproduct in the S_1 state. These triplet states may have lifetimes several orders of magnitude longer than the S_1 state and are also expected to have a significantly reduced energy barrier for chemical reaction not unlike that for the S_1 state [4].

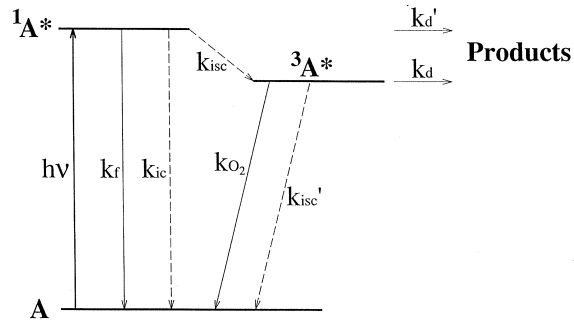

Fig. 1. Simplified scheme of molecular states of a typical molecule A and main modes of transitions between them.

To a first approximation we may represent the photon-assisted thermal incineration process of a molecule A by a model consisting of a simple competition between the thermal destruction, reaction (1) and the destruction of an electronically excited metastable state of species A (here presumed to be the triplet state T_1), reaction (2):

$$A + \text{heat} \rightarrow \sum P \quad (1)$$

$$A + h\nu \rightarrow {}^3A^* + \text{heat} \rightarrow \sum P' \quad (2)$$

As long as there is no appreciable build-up of product species P and P′ which may interact with A, i.e. if there is only a small amount of conversion of reactants to products, this mechanism may well represent the rate of destruction of A as a function of temperature and light-source power density (mW cm^{-2}).

The reaction mechanism we invoke (reactions (1) and (2)) should just be regarded as a simplified framework for discussion of the exploratory results presented in this paper. Tsang and coworkers have advanced a more detailed mechanism for the incineration of polyatomic molecules based on elementary chemical kinetics at high temperatures [11,12]. Such a scheme is an ideal tool to assess from first principles the efficiency of incineration and the incinerability of polyatomic molecules under any given set of chosen conditions. The most important practical aspect of such a detailed scheme, however, lies in the predictability of the behavior of complex mixtures under incineration conditions barring any unforeseen kinetic effects such as heterogeneous processes which may be incorporated into the model at a later time. The ultimate goal of our effort has to be seen in this context as we strive to characterize the kinetic stability of complex organic molecules at moderate temperatures in the presence of UV photons.

Two important parameters are used often when characterizing the efficiency of the destruction. For one, they are the DRE defined by

$$\text{DRE} = 100 \times \frac{\#_{\text{in}} - \#_{\text{out}}}{\#_{\text{in}}} \quad (3)$$

and the fraction remaining (f_r) defined by

$$f_r = \frac{\#_{\text{out}}}{\#_{\text{in}}} \quad (4)$$

where $\#_{in}$ and $\#_{out}$ are the number of molecules in a given volume (number density) entering and leaving the reactor, respectively, under constant flow and temperature conditions.

To determine the efficiency of UV photons in the destruction of the organic molecule we define a destruction enhancement factor R given in Eq. (5)

$$R = \frac{f_r(0)}{f_r(h\nu)} \tag{5}$$

At each given temperature two measurements are required: the first performed in the absence of UV light to obtain the fraction of the species remaining $f_r(0)$ for the pure thermal process, and the second measured in the presence of UV photons at the same temperature which gives the fraction remaining $f_r(h\nu)$ for the combined photon-assisted thermal process (see below). The values of f_r are determined by taking the ratio of the quantity of sample leaving the reaction cell after either thermal or photon-assisted thermal treatment to the quantity of the species flowing into the tubular reactor. The photon-assisted destruction occurred under irradiation of the gas phase using a pulsed excimer laser or a continuous arc discharge lamp propagating along the axis of the cylindrical flow cell.

R is the value of the enhancement factor of photon-assisted thermal versus thermal destruction, while the DRE only gives information about the change between the initial and the final concentration of each reaction separately.

In order to use the simple model shown above we introduce the competition between the thermal destruction of the ground state A, reaction (1), and the T_1 state of A (reaction (2)), but neglect the direct S_1 decomposition via k_d' due to the short S_1 lifetime (Fig. 1). We may write for the number density $\#_A$ of molecules A the thermal reaction (1) and the photon-assisted reaction (2) as rate laws (6) and (7), respectively:

$$\frac{d\#_A}{dt} = k_{th}\#_A \tag{6}$$

$$\frac{d\#_A}{dt} = (k_{th} + I\sigma\phi)\#_A \tag{7}$$

where k_{th} is the rate constant for thermal decomposition, I is the photon flux of the UV radiation at a given wavelength λ, t is the independent variable, σ is the absorption cross section and ϕ is the overall quantum yield for decomposition via the triplet state. When we integrate these two equations and take the ratio we obtain a linear relationship between ln R and the light intensity in a semilogarithmic representation according to Eq. (8):

$$R(I(\lambda),T,t) = \frac{f_r(0,T,t)}{f_r(I,T,t)} = \exp\left(I(\lambda)\sigma(\lambda,T)t'\phi(I,T)\right) \tag{8}$$

where t' is the duration of the UV illumination, either pulsed (laser) or continuous (lamp).

In a further extension to the simple model shown schematically in Fig. 1 we may express the overall quantum yield as

$$\phi(I,T) = \phi_{isc}\phi_d \tag{9}$$

where the quantum yield for intersystem crossing ϕ_{isc} from singlet to triplet state is

$$\phi_{isc} = k_{isc}/(k_{isc} + k_f + k_{ic}) \tag{10}$$

and the quantum yield for destruction is

$$\phi_d = k_d/(k_d + k_{isc}' + k_{O_2}[O_2]) \tag{11}$$

In these expressions k_{isc}, k_f, k_{ic} and k_d are the rate constants of intersystem crossing, fluorescence, internal conversion and destruction, k_{O_2} is the second-order rate constant for the oxygen quenching reaction and $[O_2]$ is the oxygen concentration, all shown schematically in Fig. 1. As will be seen later in Section 4 for pyrene and 1-bromopyrene, ϕ_{isc} is of great importance for efficient destruction. In this paper we will present results for the overall quantum yield ϕ as a function of temperature and laser power. A similar model has been presented by Graham and Dellinger [3].

The simple model (Eq. (8)) states that the branching ratio between both pathways, reactions (1) and (2), is dependent on the light dose It' corresponding to the total number of photons dispensed. The overall rate process is thus a superposition of two reactions, one of which (reaction (1)) is independent of the photon flux of the light source. From our decomposition experiments we determine the two values for f_r to evaluate R as given in Eq. (8). All the parameters shown in Eq. (8) are known except σ and ϕ, which are required for predictions using the simple model. In order to gain insight into the details of the relevant photophysical and photochemical processes we need to study the dependence of the overall quantum yield ϕ on temperature, UV light intensity and other important parameters by using experimentally determined values for R and solving for $\phi(I,T)$. Therefore, we have to know the absorption spectrum at elevated temperatures between 200 and 400 nm. For anthracene, pyrene and 1,2,4-trichlorobenzene there are published gas-phase spectra in the literature [13–18] with either no temperature dependence at all or too small a temperature range and in an inappropriate wavelength range. The almost complete lack of pertinent absorption data made us decide to measure absorption spectra of the five title compounds at elevated temperatures in the wavelength range of interest in an auxiliary study. The data of this study in the range of 150 to 650 °C are published elsewhere [19].

3. Experimental setup

We built a modular system with the purpose of conducting the main study on the photon-assisted thermal destruction as well as the auxiliary study on the absorption spectroscopy of the title compounds at elevated temperatures. For the destruc-

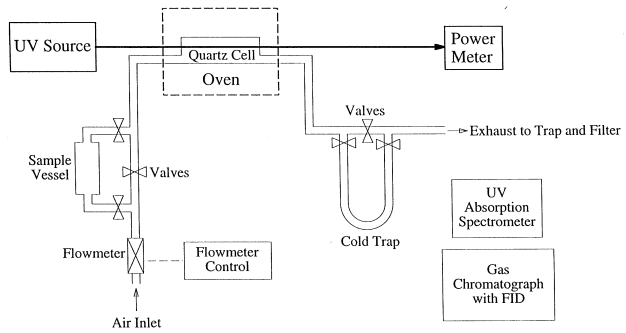

Fig. 2. Experimental setup of the laboratory-scale laser-assisted incineration experiment.

tion study the experimental setup consists of a tubular oven which may be illuminated in axial direction with photons of a UV light source, either a lamp or a laser. The lamp we used was a 200 W Hg(Xe) mixed-gas high-pressure arc lamp (Ushio, housing from AMKO equipped with a parabolic mirror, A1000) which emits about 17.2% of light intensity in the wavelength range 200–400 nm. The excimer lasers are either rare gas halide lasers operating on KrF (Lumonics model 527) emitting at 248 nm or XeCl (Spectra Physics, EMG 201 MSC) emitting at 308 nm.

The absorption cell is an all-quartz tube with a length of 50 cm and an internal diameter of 35 mm placed inside the tubular oven (Heraeus, Ro 4/50). It is connected to a heated gas supply system. The vapors of anthracene (Aldrich, 98+%), xanthone (Fluka, >97%), pyrene (Aldrich, 99+%), 1-bromopyrene (Aldrich, 99%) and 1,2,4-trichlorobenzene (Fluka, >99%) are entrained in an inlet stream of filtered compressed air which flows through the sample vessel at a known flow rate (Fig. 2). It contains either a solid sample coated on Raschig rings in order to increase the sample surface for faster evaporation or a liquid sample such as 1,2,4-trichlorobenzene. Owing to the generally low volatility of the investigated compounds used in this study the sample is heated in order to increase its vapor pressure and therefore to obtain sizable optical densities. The temperature of the sample vessel is kept constant by coiled heating wires that are connected to a proportional temperature (PID) controller. For 1,2,4-trichlorobenzene the sample vessel was cooled down using a temperature stabilized bath. The vapor concentration of these organic compounds may be estimated by the sample's vapor pressure at the temperature of the sample vessel, its rate of evaporation and the flow of compressed air, but we preferred to determine the concentration using a direct method (see below). The flow rate can be set at the entrance of the gas-inlet system using a mass flowmeter to values up to 6 $dm^3\ min^{-1}$ at ambient temperature. The setting of the flow rate determines the residence time (t_R) of the molecules in the absorption cell, typically a few to tens of seconds. In order to avoid condensation of the sample vapor on any cold spot of the internal surface we heat the transfer lines and the oven to a temperature at least 30 °C higher than the sample vessel. Therefore, we are restricted to measurements at temperatures higher than 100 °C for 1,2,4-trichlorobenzene, 200 °C for 1-bromopyrene and 150 °C for the remainder of the compounds. All the temperatures are measured using type K thermocouples.

In order to avoid the build-up of a concentration gradient due to the finite thermal accommodation in the absorption cell the sample was admitted through a 8 cm long quartz tube of 4 mm diameter located in the tubular oven thus preheating the sample. The gas phase residence time in this narrow admission tube was typically a few to 10 ms and was therefore negligible compared with the gas residence time in the main cylindrical reactor.

In order to measure the sample concentration c we collect the sample for one minute in a trap cooled to −78 °C downstream of the absorption cell (c.f. Fig. 2). Subsequently, we dissolve the trap's content in hexane (UV quality) and determine the spectrum of that solution using a common dual beam UV spectrometer (Uvikon 860) using a 1 cm quartz cuvette. The mass of the sample could now be calculated by comparing the measured optical density with solution spectrophotometric data [20,21]. We also compare the sample mass with the results that were taken from the same sample solution obtained from calibrated chromatograms measured using a gas chromatograph (GC) (Varian 3400) equipped with a flame ionization detector (FID). At higher degrees of sample decomposition ($f_r < 0.5$) we determined the mass by GC only as the UV spectrometry may not be used owing to overlapping of the sample spectrum with the spectra of products. In case of even higher extents of destruction, generally for $f_r < 10^{-3}$ and depending on the particular compound and initial concentration, f_r was determined using GC by concentration of the liquid-phase sample by solvent evaporation and prolonged sample collection (up to 1 h). Subsequently, an aliquot was injected into the GC for analysis. This led to a dynamic measurement range in f_r of about 10^5 depending on the initial species concentration.

For GC analysis we injected 1.0 μl of the solution of the collected sample and separated the different compounds (hexane, sample and reaction products) using a 30 m long PTE-5 capillary column (Supelco, 0.32 mm diameter, 0.25 μm bonded phase) together with an appropriate GC temperature program. We kept the column temperature constant to a value of 79 °C for the first 2 min and started to vent the injector after 1 min. Subsequently, the temperature of the column was increased at a rate of 20 °C min^{-1} until the sample was detected.

The chromatogram was plotted on paper by a x–t recorder and the amplitude of the peak corresponding to the investigated compound was determined. This led to great difficulties of identifying a small peak in a crowded sequence of peaks corresponding to destruction products at the highest destruction rates.

4. Results and discussion

4.1. Temperature dependence of f_r

In this section we will present the destruction behavior of the title compounds with varying temperature, photon intensity and wavelength. The gas flow rate has been set to 2 $dm^3\ min^{-1}$ at constant atmospheric pressure. We have estimated the measurement errors for small sample destruction rates to be less than 20%, due mainly to the sample collection procedure and the determination of the amount of the sample in solution. The error increases with increasing destruction rates. In some cases it can reach values on the order of a factor of two when approaching the detection limit. 1-bromopyrene represents an exception with errors that are about a factor of 2 higher compared with other compounds (see below).

In a first set of measurements we have investigated f_r as a function of temperature for the pure thermal and the combined UV photon-assisted thermal decomposition. We have chosen a modest laser power in order to ensure a stable laser output energy and to take advantage of a wide dynamic measurement range. The lamp output could not be varied and the total power measured at the end of the experiment (Fig. 2) was approximately 160 mW cm^{-2} of which 17.2%, that is approximately 27.4 mW cm^{-2}, are in the wavelength range lower than 400 nm.

We present the destruction of anthracene in terms of the fraction remaining (f_r) as a function of temperature in Fig. 3. Two sets of curves are shown, one with and the other without photons, measured at 248 nm and with the Hg(Xe) arc lamp at different concentrations using the GC method for analysis. A significant effect may already be observed in the absence of photons for the pure thermal destruction when comparing the destruction at three concentrations of 99.1, 375.5 and

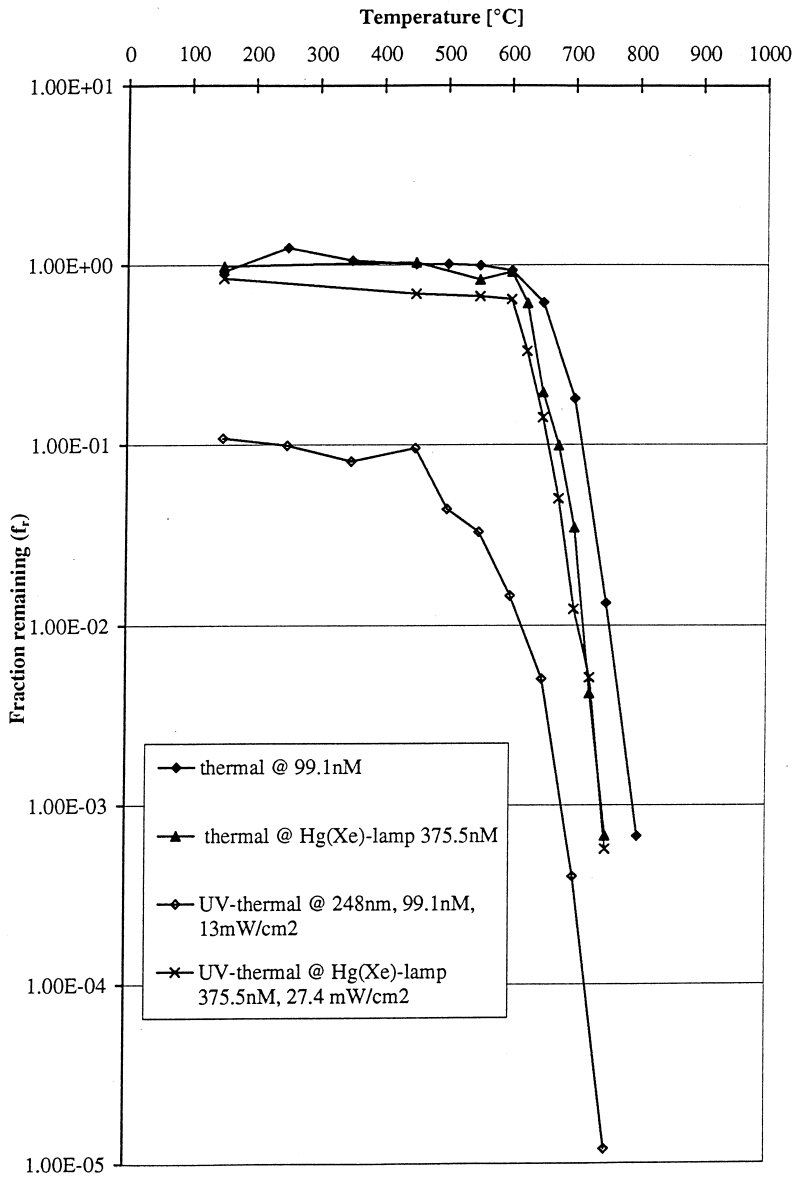

Fig. 3. Pure thermal vs. combined photon-assisted/thermal destruction of anthracene. The concentrations in the insert of the Figure refer to 20 °C. The intensity of the lamp is calculated for the wavelength range 200–400 nm only.

Table 1
Dependence of the overall quantum yield ϕ on the temperature at constant laser power

Anthracene [a]		Xanthone [b]		Pyrene [c]		1-Bromopyrene [d]		1,2,4-Trichlorobenzene [e]	
Temperature (°C)	$\phi(T)$	Temperature (°C)	$\phi(T)$	Temperature (°C)	$\phi(T)$	Temperature (°C)	$\phi(T)$	Temperature (°C)	$\phi(T)$
150	0.20	150	0.05	450	4.1×10^{-5}	250	0.10	100	2.13
250	0.21	350	0.05	600	7.2×10^{-4}	350	0.18	300	0.56
350	0.18	450	0.12	750	4.9×10^{-3}	500	0.29	400	0.98
450	0.16	550	0.33			600	0.40	500	0.82
500	0.21	600	0.42			650	0.41	550	1.28
550	0.23	650	0.57			700	0.43	600	1.27
600	0.29	675	0.80			750	0.43	650	2.17
650	0.32	700	1.01					675	3.85
700	0.40	725	1.39					700	7.42
750	0.45	750	1.19					725	6.46
		775	1.44					750	0.23
		800	2.15					775	0.19

[a] Measured at a wavelength of 248 nm, a concentration of 99.1 nM at 20 °C and a laser power of 13.3 mW cm^{-2}.
[b] Measured at a wavelength of 308 nm, a concentration of 1.19 μM at 20 °C and a laser power of 13.3 mW cm^{-2}.
[c] Measured at a wavelength of 308 nm, a concentration of 396 nM at 20 °C and a laser power of 13.3 mW cm^{-2}.
[d] Measured at a wavelength of 248 nm, a concentration of 622 nM at 20 °C and a laser power of 45.5 mW cm^{-2}.
[e] Measured at a wavelength of 248 nm, a concentration of 20.24 μM at 20 °C and a laser power of 57.6 mW cm^{-2}.

1916.3 nM, the latter of which is shown in Ref. [10]: The higher the concentration the more efficient is the pure thermal destruction at temperatures above 600 °C pointing towards the importance of secondary reactions occurring at higher concentrations [11,12].

The most important effect is the increased destruction rate which can be observed when illuminating the sample with UV photons at 248 nm, presumably owing to the large absorption coefficient of anthracene at this wavelength. At 150 °C we already observe a destruction corresponding to $f_r(h\nu) \approx 0.1$, and $f_r(h\nu)$ continuously decreases reaching a photon-enhancement factor R of more than 1000 at 750 °C. In contrast, there is only a small effect at 308 nm not exceeding the error limits [10], presumably because of the rather small absorption coefficient at 308 nm in the temperature range of interest. The destruction enhancement obtained using the Hg(Xe) lamp yields a R factor of 2.8 at 700 °C, but at still higher temperatures the effect of the photons on f_r decreases. The lamp does not emit a sufficient number of photons that overlap with the absorption of the ^{1}B band centered at 237 nm [19]. The analytical detection limit for anthracene at an initial concentration of 99.1 nM achieved in this work is determined to be approximately 10 ppm.

The overall quantum yields $\phi(T)$ determined using the measured enhancement factors together with the measured and extrapolated absorption data according to Eq. (8) are generally increasing with increasing temperature (Table 1). At the laser wavelength of 248 nm and a laser power of 13 mW cm^{-2} we determine a value of $\phi(T)$ of 0.20 at 150 °C and of 0.45 at 750 °C.

Fig. 4 shows the dependence of the fraction remaining as a function of temperature for xanthone. When taking the pure thermal-destruction curve as a reference we notice a significant decrease in f_r at 308 nm and a laser power of 13 mW cm^{-2}. f_r decreases even more for a laser power of 34 mW cm^{-2}, as expected. An even larger DRE is observed at 248 nm and 13 mW cm^{-2}, which may be due to the larger absorption coefficient at 248 nm compared with 308 nm. If anthracene and xanthone are compared at 248 nm, the scaling follows the absorption cross section, as expected from Eq. (8). We reach an enhancement of approximately 200 at 775 °C and attain the detection limit of $f_r \approx 5$ ppm for an initial concentration of xanthone of 1.19 μM. The shape of the curve describing $f_r(T)$ for UV lamp irradiation follows different profile compared with the laser destruction (Fig. 4): f_r is rather large at 150 °C but drops off quite quickly with a continuous increase of temperature. For temperatures between 500 and 700 °C the destruction using the lamp is even more efficient than the destruction at 248 nm. However, for temperatures higher than 650 °C we observe an unexpected shoulder in the destruction curve. This was probably caused by a product of the photon-assisted thermal destruction that had a GC retention time identical to xanthone and could therefore not be determined properly.

The quantum yields for xanthone have been determined in three different measurement series. The $\phi(T)$ are rising continuously with temperature (Table 1). The values lie between 0.17 at 150 °C and 1.7 at 775 °C for a laser power of 13 mW cm^{-2} at 248 nm, between 0.05 and 2.15 and 0.06 and 1.6 for laser powers of 13 and 34 mW cm^{-2}, respectively, at 308 nm. For high temperatures, mostly above 700 °C and small laser power the overall quantum yield is exceeding unity. Generally, a value of $\phi(T)$ larger than unity points towards the occurrence of a photon-initiated chain reaction. In our measurements we obtain values larger than 1.4 under several conditions.

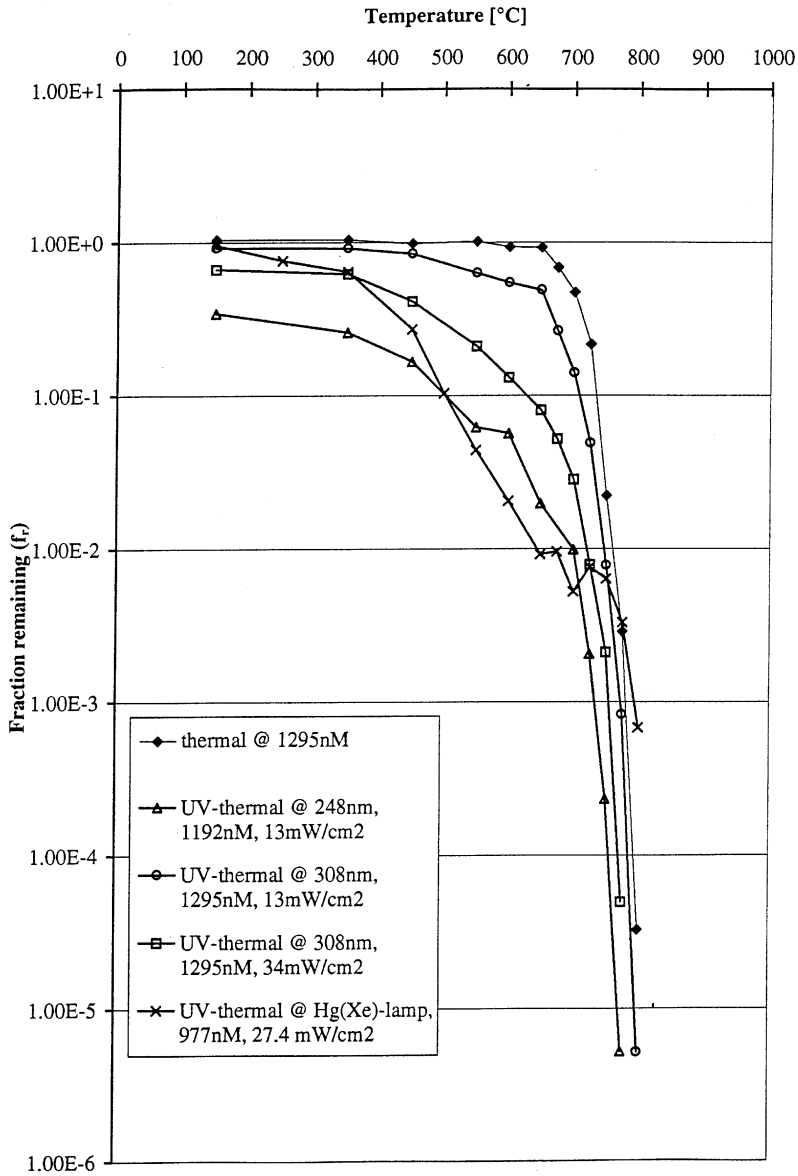

Fig. 4. Pure thermal vs. combined photon-assisted/thermal destruction of xanthone. The concentrations in the insert of the Figure refer to 20 °C. The intensity of the lamp is calculated for the wavelength range 200–400 nm only.

Fig. 5 shows the photon-assisted thermal destruction of pyrene in terms of $f_r(T)$. Surprisingly, we observe hardly any measurable R at a wavelength of 308 nm and a laser power of 45.5 mW cm^{-2}, except at a temperature of 725 °C where R equals 2. Using the UV lamp we observe a slight destruction enhancement to result in a limiting value of $R=4.7$ at high temperatures. This is a surprisingly small value for R as pyrene has a high absorption coefficient at wavelengths lower than 340 nm, for instance 26 000 $dm^3\,mol^{-1}\,cm^{-1}$ at 308 nm [19]. Therefore, we had expected large values for R compared with xanthone, for instance. The measured quantum yield is therefore rather small, increasing with temperature as for the other compounds, with values of 4.1×10^{-5} to 4.9×10^{-3} for 450 and 700 °C, respectively (see Table 1).

Fig. 6 shows the destruction of 1-bromopyrene in terms of $f_r(T)$. In contrast to pyrene we observe a large effect of the UV photons on the extent of the destruction. Already at a temperature of 250 °C we notice $R=8$ at 308 nm even though the absorption coefficient for 1-bromopyrene at this wavelength, 8450 $dm^3\,mol^{-1}\,cm^{-1}$, is a factor of three smaller than for pyrene. R increases continuously up to $R=64$ at 650 °C. The enhancement due to the presence of photons of a Hg(Xe) lamp is enormous leading to $R=475$ at 250 °C which means that only 0.2% of the initial molecules leave the flow reactor undissociated at this modest photon flux. The efficiency of destruction increases continuously reaching its peak value at 700 °C with $R=6115$. The overall quantum yield increases with temperature from 0.10 to 0.43 between 250 and 750 °C (Table 1).

We thus obtain a significant improvement of efficiency of destruction for 1-bromopyrene compared with pyrene, although the former has a considerably smaller absorption at

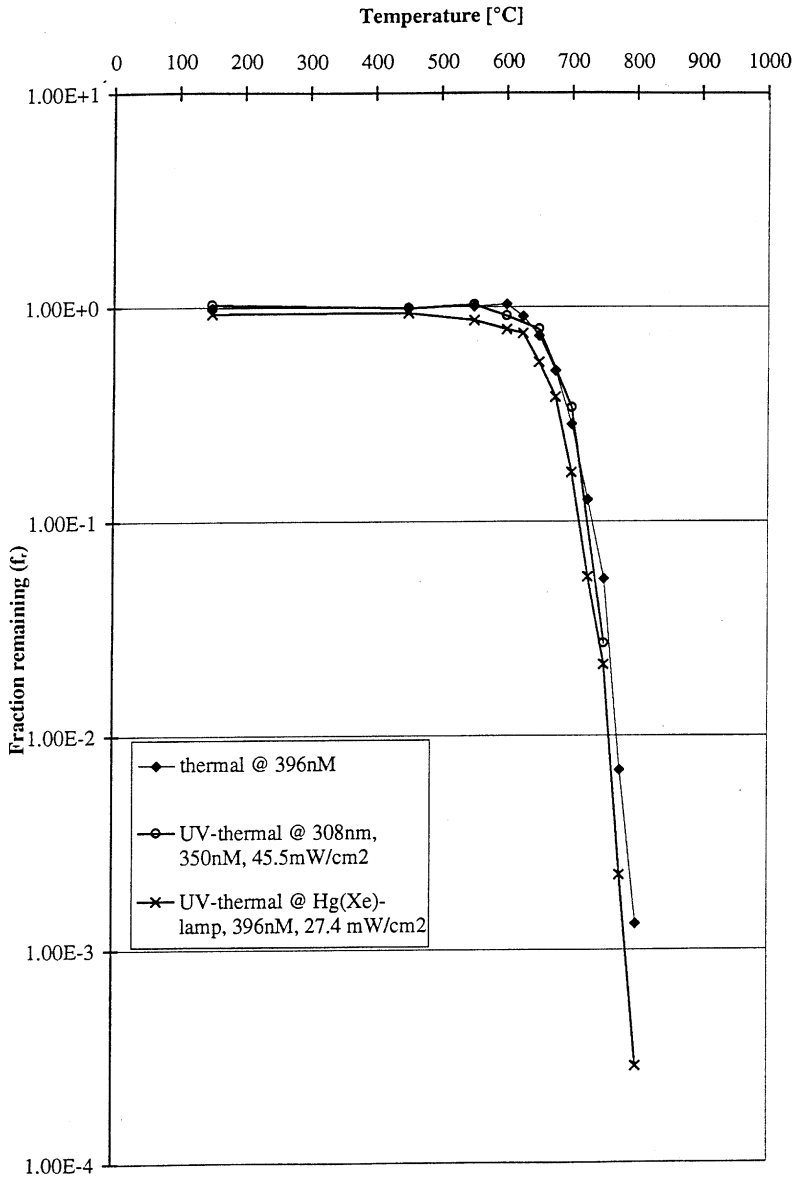

Fig. 5. Pure thermal vs. combined photon-assisted/thermal destruction of pyrene. The concentrations in the insert of the Figure refer to 20 °C. The intensity of the lamp is calculated for the wavelength range 200–400 nm only.

308 nm as well as over the whole UV spectrum from 200 to 400 nm. From the published data on rate constants for fluorescence, intersystem crossing and phosphorescence of Barradas et al. [22] for pyrene and 3-bromopyrene (the one we use is 1-bromopyrene) determined at 77 K we may gain some insight. The comparison between pyrene and its 3-bromo derivative reveals an internal heavy atom effect [23]. This becomes apparent as the rate constant for intersystem crossing k_{isc} for 3-bromopyrene is larger by a factor in excess of 400 than that for pyrene, while the rate constant for the decay of the fluorescence k_f is only larger by a factor 7.8 when comparing 3-bromopyrene with pyrene. Neglecting the rate constant for internal conversion k_{ic} (Fig. 1) as is done quite frequently [23], we may calculate from the data of Barradas et al. [22] the quantum yields for intersystem crossing ϕ_{isc} to be 0.09 for pyrene and 0.83 for 3-bromopyrene. The value for pyrene may be compared with published values [23,24]. As an example, Birks [23] determined ϕ_{isc} values for pyrene in several solutions and at various temperatures to be between 0.18 and 0.38. If we use a representative value of $\phi_{isc} = 0.28$ (average) we obtain k_{isc} of 530 000 s^{-1} for pyrene, a value larger than the one given by Barradas [22]. The k_{isc} of 3-bromopyrene is still larger by a factor of 100 when compared with the above value of k_{isc} of pyrene. It follows that the theory in its simplest form of Eq. (8) has to be extended in terms of Eq. (9) in order to take into account differences in ϕ_{isc}. If fundamental data on ϕ_{isc} as a function of temperature were known we would be able to separate ϕ_{isc} from ϕ_d thus permitting more precise predictions.

As an additional result we observed that 1-bromopyrene is more stable than pyrene as far as the pure thermal destruction is concerned.

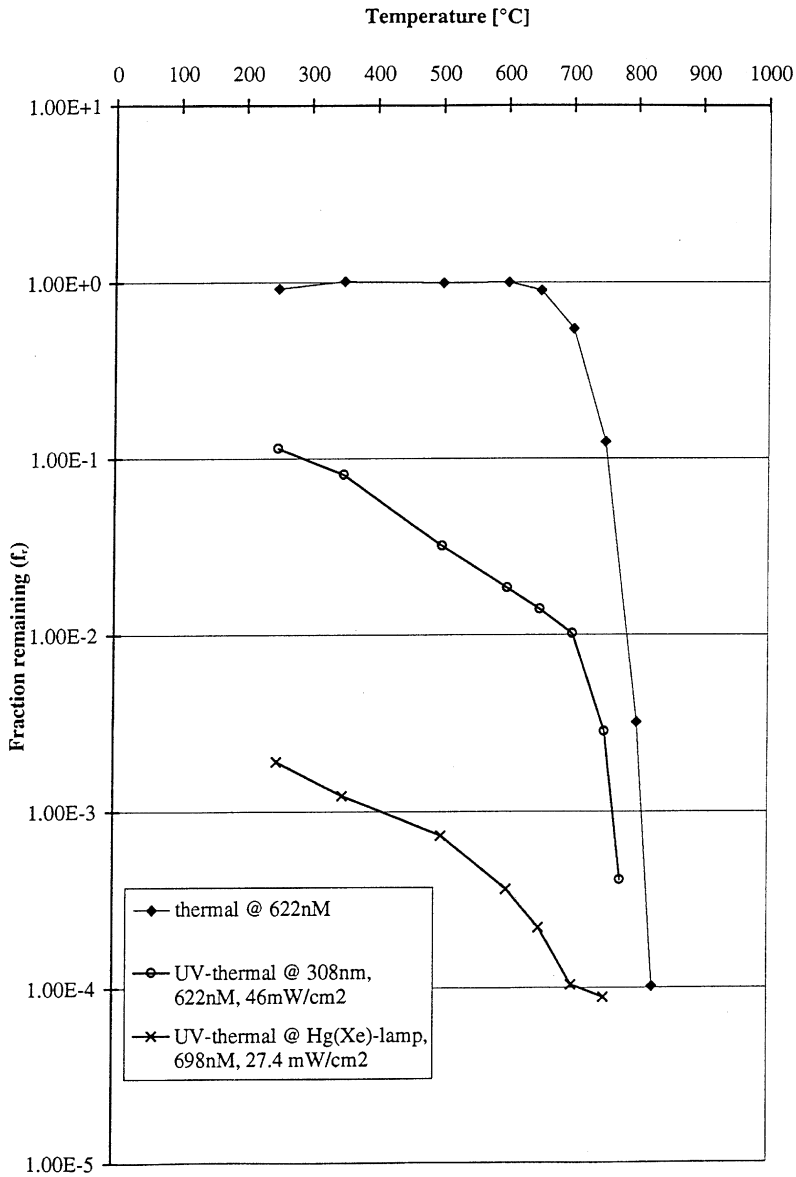

Fig. 6. Pure thermal vs. combined photon-assisted/thermal destruction of 1-bromopyrene. The concentrations in the insert of the Figure refer to 20 °C. The intensity of the lamp is calculated for the wavelength range 200–400 nm only.

We admit that the GC/FID technique encountered many problems for the quantitation of 1-bromopyrene. Therefore, we performed many measurements in order to confirm the given results. Despite the large number of samples the error limits on 1-bromopyrene are about a factor of 2 higher than for the other compounds owing to difficulties of the analytical procedure for this compound.

Fig. 7 shows f_r of 1,2,4-trichlorobenzene as a function of temperature. Owing to the rather small absorption at 248 nm we observe only a small value of R at low temperatures, e.g. $R = 1.1$ at 300 °C and 13 mW cm^{-2}. However, a value of approximately 40 has been obtained at 750 °C and a laser power of 13 mW cm^{-2}. We observe the merging of the two curves, $f_r(0)$ and $f_r(h\nu)$, at temperatures above 750 °C which may be explained by the fact that we are close to the detection limit of our analytical system thus leading to increased errors because of possible evaporation of the high volatility tri-substituted benzene. Therefore, we think that this result is more of an analytical artifact than a significant trend, the more so as a similar behavior could not be observed at the higher laser power of 57 mW cm^{-2}. In the latter experiment the detection limit of approximately 1 ppm of the starting concentration of 20.2 μM was reached already at 725 °C. However, we observe a R factor of approximately 7700 at 700 °C and a laser power of 57 mW cm^{-2}. The lamp irradiation is causing larger destruction than laser irradiation at 248 nm and 13 mW cm^{-2} at low temperature. At higher temperatures f_r(lamp) approaches the values for 248 nm, except for the artifact of the data above 725 °C (see Fig. 7).

The two sets of overall quantum yields determined from the measurement at 248 nm show the same trend as for the other compounds (Table 1). However, we observe values for

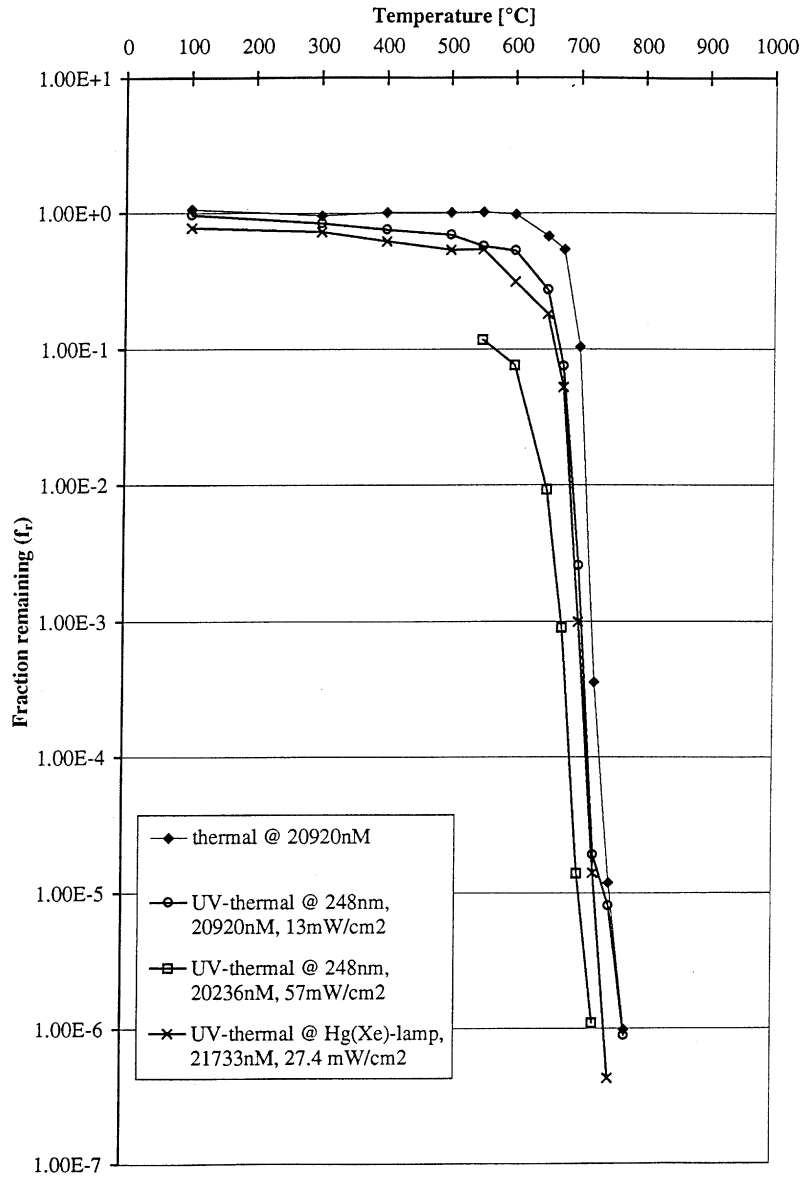

Fig. 7. Pure thermal vs. combined photon-assisted/thermal destruction of 1,2,4-trichlorobenzene. The concentrations in the inset refer to 20 °C. The intensity of the lamp is calculated for the wavelength range 200–400 nm only.

$\phi(T)$ that are exceeding unity by a large margin. $\phi(T)$ was found to be in the range of 0.56 at 300 °C up to 7.42 at 700 °C for 13 mW cm^{-2} laser power. For 57 mW cm^{-2} we measure a range of 1.18 at 550 °C to 4.10 at 700 °C. For the higher laser power the quantum yield ϕ decreases compared with small laser power.

From the measurements on anthracene, xanthone and 1,2,4-trichlorobenzene we may conclude that the photon-assisted destruction at 308 nm using the XeCl laser is less efficient than for the two other light sources, presumably because of the less favorable spectral overlap of the light source emission with the absorption spectrum of the compound. A ranking between the lamp and the KrF laser at 248 nm is not possible because it depends on the compound to be measured. For all five compounds the Hg(Xe) lamp shows efficient destruction due to important overlap of the emission of the lamp and the absorption spectrum of the compound. This is an important result for future applications in industrial emission controls or in incinerators. For industrial applications it is still advantageous to work with lamps instead of lasers for operating reasons. In addition, the intensity of the lamp may be increased by selecting a more powerful lamp in order to increase *R*, but in contrast to a laser the scale-up may involve lower cost (investment and operating costs). In an industrial application the spectrum of an unknown compound in the gas stream will almost certainly overlap with the emission spectrum of the lamp.

As we set the gas flow at room temperature it rises inside the heated reactor cell with increasing temperature owing to the expansion of the gas. The gas expansion decreases the actual concentration of the sample molecules in the cell and simultaneously increases the gas flow thus causing a reduc-

tion of the residence time. These two effects are not affecting our measurements as we are interested in the relative enhancement at a fixed temperature. However, when comparing different temperatures one has to keep in mind this additional ''hidden'' parameter as a longer residence time causes a larger extent of destruction, both with and without photons. When data such as displayed in Figs. 3–7 are normalized to the ambient temperature residence time or concentration the precipitous drop of f_r with increasing temperature would be even more pronounced.

From two series of measurements of $f_r(0)$ and $f_r(h\nu)$ as a function of temperature we determined an apparent activation energy E_a of 157.4 kJ mol^{-1} for the pure thermal and 69.5 kJ mol^{-1} for the UV enhanced thermal destruction of anthracene at temperatures higher than 650 °C (99.1 μM). For xanthone we found 222.3 kJ mol^{-1} and 111.9 kJ mol^{-1} and for 1,2,4-trichlorobenzene 331.5 kJ mol^{-1} and 233.9 kJ mol^{-1}, respectively. These values were derived by assuming a first order rate law for the disappearance of the molecular species. From the measurement of anthracene (Fig. 3) it became clear, however, that the rate of thermal destruction follows a more complex rate law because the rate constant k derived from the relation

$$\#_A(t) = \#_A(0)\ \exp(-kt) \qquad (12)$$

where $f_r(0) = \#_A(t_R)/\#_A(0)$ depended both on the concentration as well as on the residence time t_R. Nevertheless, the values for k that were used to compute the activation parameters were obtained at low concentrations and for short residence times in order to keep the extent of secondary chemistry to a minimum. The values for E_a quoted above therefore do not pertain to the elementary unimolecular decomposition of the species and merely serve to point out the overall temperature sensitivity of the rate of species destruction under our experimental conditions.

The density distribution inside the reaction cell can not easily be determined. We only measure the total number of molecules at the entrance and exit of the reactor and can calculate the residence time from the known air flow at ambient temperature corresponding to the volume of air swept across the reactor. Only under the assumption of a unimolecular decomposition are we able to determine the density profile inside the cell.

4.2. Power dependence of f_r

In more detailed experiments we investigated the dependence of the photon-enhancement factor R on the average laser power at 248 nm for anthracene, xanthone and 1,2,4-trichlorobenzene. Surprisingly, for all compounds a similar shape of the curve was observed which was unexpected following the simple model (Eq. (8) or (9)). Instead of a straight line in a semilogarithmic plot we obtain curves in which R seems to reach asymptotic values (see Figs. 8–10). For small values the laser power dependence seems to correspond to a straight line but for higher powers all curves are turning towards less than the expected R values. If we linearly extrapolate taking the R values of xanthone as an example (see below) at values smaller than 30 mW cm^{-2} at 248 nm, we may expect a value on the order of 100 000 at 70 mW cm^{-2} instead of the measured value of about 1000.

As an explanation we exclude triplet energy pooling corresponding to the deactivation of two excited T_1 molecules going to S_0 and a highly excited singlet state because R is independent of the sample concentration, thus of the triplet density (see Figs. 8 and 9). There does not seem to be an effect of the pulse repetition rate of the laser at constant power as well. This smaller than expected value of R at higher laser power density is most probably caused by partial illumination of the heated cell owing to the shadowing effect of the transfer

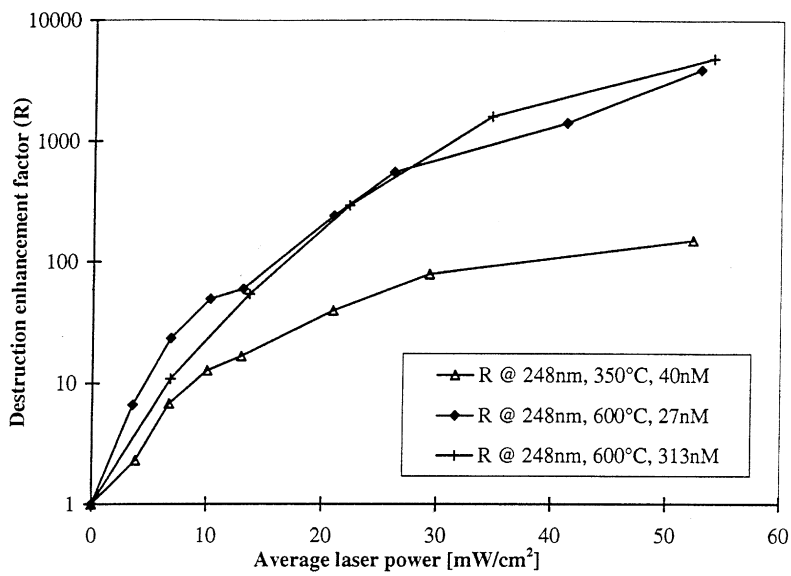

Fig. 8. Dependence of the destruction enhancement factor R on the laser power for anthracene at 350 °C and at 600 °C for two different concentrations and residence times of 6.7 s and 4.8 s, respectively.

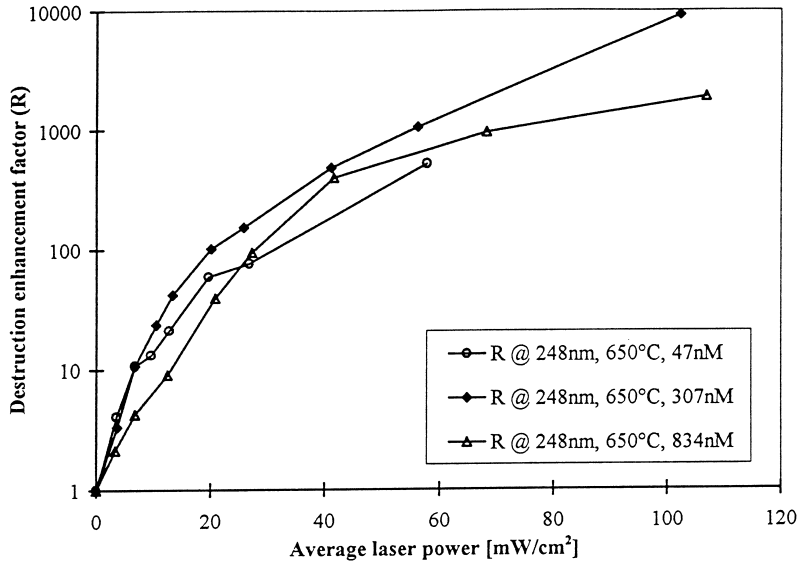

Fig. 9. Dependence of the destruction enhancement factor *R* on the laser power for xanthone at 650 °C for three different concentrations and a residence time of 4.5 s.

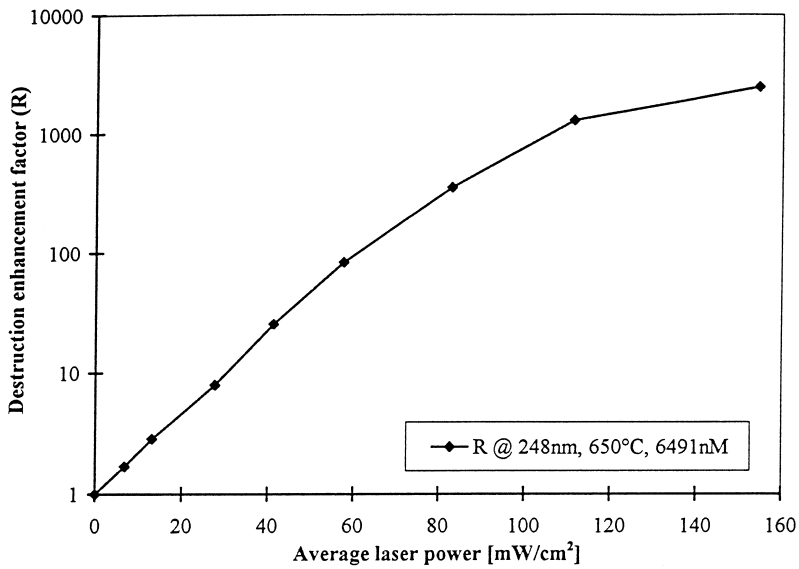

Fig. 10. Dependence of the destruction enhancement factor *R* on the laser power for 1,2,4-trichlorobenzene at 650 °C and a residence time of 4.5 s.

lines. Presently, the transfer lines cover approximately one third of the cell's cross section. If only traces of the sample would flow across the cell without being illuminated by the laser pulses this could well explain the deviation from the expected linearity.

The destruction efficiency enhancement *R* for anthracene as a function of average laser power at 350 °C and at two different concentrations at 600 °C for 248 nm irradiation is presented in Fig. 8. At 600 °C we determine an enhancement of approximately 400 at the applied laser power of 53 mW cm^{-2} and at a residence time of 4.8 s and concentrations of 27.2 nM and 312.5 nM. Even with the shadowing of the cell discussed above we reach a *R* value of about 150 at a temperature of 350 °C using an average laser power of 52 mW cm^{-2} at a residence time of 6.7 s. The measured quantum yields $\phi(I)$ at 350 °C are continuously decreasing from 0.27 to 0.089 when increasing the laser power from 6.7 mW cm^{-2} to 52.3 mW cm^{-2} (Table 2). At 600 °C the $\phi(I)$ values are again decreasing from 0.50 to 0.15 with an increase of the laser power from 3.5 mW cm^{-2} to 52.8 mW cm^{-2} at a concentration of 27.2 nM. However, this decrease is independent of the concentration.

We have measured *R* for xanthone at three different concentrations at 650 °C and 248 nm, but there seems to be no marked dependence on concentration (Fig. 9) in analogy to anthracene. Only for high average laser powers we observe a discrepancy in *R* of a factor 5 between the two concentrations at 103 mW cm^{-2} and a residence time of 4.5 s leading to destruction efficiencies of ca. 9100 and 1800 at concentrations of 307.3 and 834.4 nM, respectively. The quantum yields for the three concentrations may be summarized as they show the same trend with similar values. In conclusion,

Table 2
Dependence of the overall quantum yield ϕ on the laser power at constant temperature

Anthracene [a]		Xanthone [b]		1,2,4-Trichlorobenzene [c]	
Laser power (mW cm^{-2})	$\phi(I)$	Laser power (mW cm^{-2})	$\phi(I)$	Laser power (mW cm^{-2})	$\phi(I)$
3.5	0.50	3.6	1.33	6.8	2.15
6.8	0.43	6.7	1.41	13.1	2.23
10.2	0.35	10.5	1.20	27.7	2.07
13.1	0.29	13.3	1.12	41.3	2.18
20.9	0.24	20.1	0.92	57.6	2.13
26.1	0.22	25.8	0.78	83.0	1.96
41.1	0.16	41.1	0.60	111.4	1.78
52.8	0.15	56.3	0.49	154.6	1.40
		102.3	0.36		

[a] Measured at a temperature of 600 °C, a wavelength of 248 nm, a residence time of 4.8 s and a concentration of 27 nM.
[b] Measured at a temperature of 650 °C, a wavelength of 248 nm, a residence time of 4.5 s and a concentration of 307 nM.
[c] Measured at a temperature of 650 °C, a wavelength of 248 nm, a residence time of 4.5 s and a concentration of 6.49 μM.

we observe a typical decrease of $\phi(I)$ from 1.41 to 0.35 for increasing laser power between 6.7 mW cm^{-2} and 102.3 mW cm^{-2} at a concentration of 307.3 nM (Table 2).

We were able study 1,2,4-trichlorobenzene up to the maximum of available laser power of about 155 mW cm^{-2} owing to the rather moderate photo-enhanced destruction of this trisubstituted benzene (Fig. 10). We also obtained a R value of approximately 2400 at 155 mW cm^{-2} and a residence time of 4.5 s. The quantum yields again show a decrease of the $\phi(I)$ values of 2.15 to 1.40 for a laser power of 6.8 mW cm^{-2} and 154.6 mW cm^{-2}, respectively. It may be to noticed that we observe values of $\phi(I)$ that exceed unity for all laser powers at 650 °C (Table 2).

5. Conclusion

We have studied the combustion (oxidation) of five polycyclic aromatic hydrocarbons, anthracene, xanthone, pyrene, 1-bromopyrene and 1,2,4-trichlorobenzene in a laboratory-scale incineration reactor illuminated with photons from either a KrF- or a XeCl-excimer laser at 248 and 308 nm, respectively, or a Hg(Xe) arc lamp. We observe a pronounced increase of DRE of the combined photon-assisted thermal relative to the thermal process. Using anthracene as an example we measure an enhancement factor R of 8.5 already at 150 °C owing to photochemistry brought about by the large absorption cross section at 248 nm. At 750 °C we reach a DRE of approximately 99.999%, our present detection limit for anthracene, and determine a photon-enhanced R in excess of 1000. Using simple theory we observed that photo-enhancement is also dependent on the absorption coefficient, but, there is at least one further internal parameter, the quantum yield of intersystem crossing to generate the lowest triplet states, responsible for the efficiency of destruction.

Owing to the photon intensity and the spectral overlap of the light source with the spectrum of the compound we conclude that the output of the XeCl laser at 308 nm is less efficient at photon-assisted thermal destruction than the two other light sources, laser illumination at 248 nm from a KrF excimer laser and lamp emission from a Hg(Xe) arc. The DRE caused by lamp and KrF laser emission at 248 nm depends on the compound and the light intensity at hand. We may summarize that the photon-enhancement factor R is the larger the higher the temperature, even if the sample residence times decreases. The increasing saturation of the R values with increasing laser power seems to be independent of the sample and is attributed to an experimental artifact.

Comparing pyrene and 1-bromopyrene we could demonstrate the importance of the quantum yield of intersystem crossing. Both compounds have about the same absorption coefficients, but 1-bromopyrene which populates the low energy triplet states faster decomposes very efficiently, whereas pyrene whose quantum yield for intersystem crossing is lower does not show a significant photo-enhancement effect on its decomposition. The quantum yield ϕ generally increases with increasing temperature but decreases with increasing laser power. We observe overall quantum yields that exceeds values of unity for xanthone and 1,2,4-trichlorobenzene.

The large measured values of DRE for photo-enhanced destruction of polycyclic aromatic compounds at modest temperatures are promising for future applications of improved incineration technology of highly toxic waste.

Acknowledgements

The authors would like to thank H. van den Bergh for his enduring support and the possibility to perform this work in his laboratory and Alfred Neuenschwander and Flavio Comino for their technical support. This work was supported by the Swiss National Science Foundation under grant no. 20-37599.93.

References

[1] OECD, OECD Environmental Data, Compendium 1993, pp. 135, 147.
[2] E.T. Oppelt, JAPCA 37 (1987) 560.
[3] J.L. Graham, B. Dellinger, Energy 12 (1987) 303.
[4] J.L. Graham, B. Dellinger, in: B.P. Gupta, W.H. Traugott (eds.), Proc. 4th Int. Symp. Solar Thermal Technology Research Development and Applications, Hemisphere Publishing Corporation, New York, 1990, p. 391.
[5] G.C. Glatzmaier, R.G. Nix, M.S. Mehos, J. Environ. Sci. Health A25 (1990) 571.
[6] J.L. Graham, J.M. Berman, B. Dellinger, J. Photochem. Photobiol. A: Chem. 71 (1993) 65.
[7] J.L. Graham, H.B. Dellinger, US Patent 5,417,825 (May 23, 1995).
[8] G. Samdani, Chem. Eng. (May 1995) 15.
[9] A. Thöny, H. van den Bergh, M.J. Rossi, Environ. Sci. Technol. 30 (1996) 1789.
[10] A. Thöny, H. van den Bergh, M.J. Rossi, in: Proc. 89th Annu. Meet. Air and Waste Management Association, June 23–28, 1996, Nashville TN, Paper 96-FA130B.06.
[11] W.M. Shaub, W. Tsang, Environ. Sci. Technol. 17 (1983) 721.
[12] W. Tsang, D. Burgess Jr., Combust. Sci. Technol. 82 (1992) 31.
[13] K.H. Härdtl, A. Scharmann, Z. Naturforschg. 12a (1957) 715.
[14] J. Ferguson, L.W. Reeves, W.G. Schneider, Can. J. Chem. 35 (1957) 1117.
[15] L.E. Lyons, G.C. Morris, J. Mol. Spectrosc. 4 (1960) 480.
[16] R.S. Dygdala, K. Stefanski, Chem. Phys. 5 (1980) 51.
[17] H. Scharping, C. Zetzsch, H.A. Dessouki, J. Mol. Spectrosc. 123 (1987) 382.
[18] W.R. Ware, P.T. Cunningham, J. Chem. Phys. 43 (1965) 3826.
[19] A. Thöny, M.J. Rossi, J. Photochem. Photobiol. A: Chem., 104 (1997) 25.
[20] H.H. Perkampus, I. Sandeman, C.J. Timmons, DMS-UV Atlas of Organic Compounds, Vols. 1–5, Butterworth, London and Verlag Chemie, Weinheim, 1966–1971.
[21] H. Conrad-Billroth, Z. Phys. Chem. (B) 19 (1932) 76.
[22] I. Barradas, J.A. Ferreira, M.F. Thomaz, J. Chem. Soc. Faraday Trans. 2 69 (1973) 388.
[23] J.B. Birks, Organic Molecular Photophysics, Vols. 1 and 2, Wiley, London, 1973.
[24] A.R. Horrocks, F. Wilkinson, Proc. R. Soc. London, Ser. A 306 (1968) 257.